Research article

X-RAY SPECTROMETRY

Received: 29 September 2015 Revised: 8 December 2015 Accepted: 5 January 2016 Published online in Wiley Online Library

(wileyonlinelibrary.com) DOI 10.1002/xrs.2683

Characterization of the VARIAN® PaxScan 2020+ flat panel detector for quantitative X-ray imaging

F. A. Geser,[a,c,d]* D. Chacón,[c,d,f] R. Figueroa,[b] F. Malano,[a,d,e] M. Santibañez[b] and M. Valente[a,b,d]

In this work, the response of the VARIAN® PaxScan 2020+ flat panel detector was characterized in terms of spatial resolution and uniformity across the detection area along with detection efficiency for photon beams from conventional X-ray tubes. This information is not commonly provided by the manufacturer. The characterization of spatial resolution, response uniformity and the detection efficiency of the VARIAN® PaxScan 2020+ are a crucial key for improving imaging procedures with diagnostic purposes, mainly when quantification by image processing is required. According to the obtained results, the VARIAN® PaxScan 2020+ detector has, on average, a spatial uniformity, considered as detector response corresponding to different positions for a fixed excitation beam, of 77% measured across the whole detection area 19.8×19.8 cm^2; whereas the minimum size measurable is (357 ± 14) μm. A rigorous method is shown to characterize the quantum efficiency, obtaining a suitable description and parameterization of the quantum efficiency as a function of energy. The incorporation of spatial uniformity and quantum efficiency for the convolution of the recorded images is in fact mandatory for the extraction of accurate quantitative information of scanned samples.

Introduction

In recent decades, the use of flat panel detectors has proliferated, replacing traditional film radiography, especially in clinical applications like bi-dimensional (2D) and tri-dimensional (3D) imaging.[1–3] The incorporation of 2D digital detectors provides important advantages for intra-operatory imaging with C-arm [4] as well as enhancements in radiotherapy.[5,6]

Quite all X-ray imaging techniques may profit the benefits of digital detectors in order to optimize the integral quality of acquired images and simultaneously reducing radiation exposure according to the As Low As Reasonably Achievable (ALARA) principle.[7] In this sense, Amorphous Silicon flat panel detectors present a clear advantage in contrast with traditional systems based on storage phosphor plates and screen-film systems.[8]

From a general point of view, solid-state detectors are characterized by their sensitive detection material consisting of a solid semiconductor (*Si*, *Ge*), which improves the interaction event occurrence because of the higher density compared with other devices.[9] This technology is based on thin scintillator layers (*CsI*(*Tl*), *NaI*(*Tl*)) that emit visible light while being irradiated, because of the presence of the *Tl* impurities that produce meta-stable electronic states.[10]

The sensitive material is a semiconductor, which generates the electrical signal collected by applying potential differences externally. The signal is then convert to digital by a pulse processor and is directly related to the number of events that occurred at each point of the scintillation layer. The visible light signal response emitted in the semiconductor is incremented using photomultiplier tubes.

The 2D detector investigated in the present study is part of the integral X-ray imaging facility at LIIFAMIR®. The flat panel is needed for quantitative analysis, such as high-resolution micro-tomography (μCT), determination of effective absorption coefficient of different biological samples through imaging, among others. In this terms, an accurate quantification of the response uniformity across the detection area, together with determination of quantum efficiency, becomes mandatory preliminary tests to characterize the flat panel that shall be part of the imaging facility.

It is well known that radiation detectors are not perfect in performing the task for which they where designed. There are always different energy ranges in which these detectors work properly, and other where they fail on their task because of reduced efficiency. Certainly, all detection properties depend on different factors according to the radiation under consideration. Some of the properties that can be measured to correct for a wide variety of effects are as follows: the spatial resolution that characterized the relationship between digital pixels and physical distances and the energy efficiency that represents

* *Correspondence to: Federico A. Geser, Institute of Physics E. Gaviola - CONICET, Córdoba, Argentina. E-mail: fgeser@famaf.unc.edu.ar*

a *Institute of Physics E. Gaviola - CONICET, Córdoba, Argentina*

b *Departamento de Ciencias Físicas, Universidad de La Frontera, Temuco, Chile*

c *FaMAF - National University of Córdoba, Córdoba, Argentina*

d *Laboratory for Research and Instrumentation in Physics Applied to Medicine and X-Ray Imaging (LIIFAMIR®), National University of Córdoba, Córdoba, Argentina*

e *National University of Río Cuarto, Córdoba, Argentina*

f *Departamento de Física, Universidad Nacional, Heredia, Costa Rica*

the relative capacity to respond to different photon energies of the incident beam. These properties give an idea of how accurate the flat panel is if one tries to obtain quantitative information from it.

During quality control of this instrument, image quality plays an important role, thus requiring a reliable verification of the spatial resolution within the field of view. In this context, it is introduced that the concept of 'minimum resolution' is defined as the size of the smallest sample that can be unequivocally resolved by the detection system. It is known that the pixel size (detector manufacturer usually gives a value of the pixel pitch) is always smaller than this measured spatial resolution because of the non-ideal nature of the real detector. There are different methods devoted to assess the minimum resolution. In this work, the implemented method is based on the well-known transfer functions, specifically the *point spread function* (*PSF*) and *modulation transfer function* (*MTF*). These are usually applied to different linear response optical systems. The use of this theoretical information of the system makes it possible to determine minimum spatial resolution in different regions of the flat panel detector.

The flat panel detector used is VARIAN® Paxscan 2020+ Amorphous Silicon Digital X-Ray Detector. It is designed for cardiovascular diagnostic by imaging and low-dose imaging. The detector's efficiency curve is not provided by the manufacturer, and it is of great importance to correct measurements in order to deliver standard magnitudes. The detector's efficiency depends on a large number of variables, such as its geometry, its detection surface, the material it is made of and the energy range of interest.

Image treatment and calculations involved were made using MatLab® [1]software.

As a result of this work, it was possible to experimentally obtain the spatial uniformity across the detection area, the minimum size measurable by the detector and the corresponding quantum efficiency curve.

Materials and methods

This section is sub-divided in order to separate theory and experimental setup with the aim of facilitating an expeditious reading.

Theoretical background

This section provides a brief description of the main issues regarding characterization of X-ray detectors. Further specific details can be found elsewhere.[9,11]

The spatial uniformity of detector response

The capacity to detect a point source constitutes a first approach for the spatial resolution of the detection system. Ideally, the obtained signal from a point source should be described by a Dirac delta function. Of course, this is not the case with real detectors.

If $f(x,y)$ is a 2D object, and an image $i(x,y)$ is obtained by a measure system $\hat{S}$, the relationship between object and image stands for $i(x,y) = \hat{S}(f(x,y))$. As a first approximation, it might be considered that the detector acts as a system having linear response,[12] so that the image is obtained by usual convolution, as indicated by expression (1):

$$\begin{aligned} i(x,y) &= \int S(x-u,y-v)f(u,v)dudv \\ &= f(x,y) \otimes S(x,y) \end{aligned} \tag{1}$$

The symbol $\otimes$ in the previous equation indicates the mathematical operation of convolution. Then, applying the convolution theorem,[13,14] the result in expression (2) is obtained in a straightforward manner:

$$\mathcal{F}(i)(u,v) = \mathcal{F}(f)(u,v) \cdot \mathcal{F}(S)(u,v) \tag{2}$$

where $\mathcal{F}$ denotes Fourier transform and $\mathcal{F}(S)(u,v)$ is the spatial frequency response of the measurement system. $\mathcal{F}(S)$ is a complex function and belongs to the family of *optical transfer functions* (*OTF*). The variables (u,v) are *spatial frequencies* usually measured in line pairs per millimeter (lp/mm) or cycles per millimeter. The *OTF* function is composed of two different transfer functions known as *MTF* and *phase transfer function* (*PTF*). Usually, the *MTF* is accepted as the normalized magnitude of *OTF*, so it can be described as indicated in expressions (3):

$$\begin{aligned} OTF(u,v) &= |OTF(u,v)|\, e^{iarg(OTF(u,v))} \\ &= |OTF(u,v)|\, e^{iPTF(u,v)} \end{aligned} \tag{3}$$

and (4):

$$MTF(u,v) = \frac{|OTF(u,v)|}{max(|OTF(u,v)|)}. \tag{4}$$

The *MTF* has a typical cutoff frequency f_0 for which the image $i(x,y)$ might be reconstructed by sampling it in a series of points (pixels) spaced at a distance given by expression (5):

$$2f_0 \geq \frac{1}{R} \tag{5}$$

This is a consequence of Nyquist–Shannon sampling theorem,[15,16] where R^{-1} might be thought of as the highest spatial frequency contained in the measurement.

In this context, the flat panel detector can be thought of as a sampling system that transforms a continuum variable into a discrete one. Considering that the minimum spatial size that can be detected by the flat panel corresponds to a cutoff spatial frequency where *MTF* becomes typical exponential decay, expression (6) can be applied for the calculation of f_0.

$$MTF(f_0) = 1/e \tag{6}$$

The smallest experimental size that can be measured is defined as R. The *MTF* value used to determine f_0 is that for which $MTF = 0$. This happens only for the asymptotic limit, because of the shape of *MTF*. Usually, values between 3% and 10% are used,[17,18] because they are related to the ability of the human eye to distinguish low contrast differences. This is why a typical exponential rate was taken as the criterion proposed to obtain the frequency, corresponding to $\sim$ 36% of *MTF* value. Thus, the minimum spatial resolution is $R \approx \frac{1}{2f_0}$. This might correspond to the pixel pitch of the detector, extended by the manufacturer, if it were a perfect detection system.

In the case of point sources, one has $f(x,y) = \delta(x)\delta(y)$, then $i(x,y) = S(x,y)$, and the image obtained is exactly the response of the system. It is known as *PSF*. This is the *OTF* that is used in this work to obtain the *MTF* and consequently the spatial resolution in different points of the detector.

[1] MATLAB® license MathWorks 3407-8985-4332-9223-7918

Characterization of quantum efficiency

Quantum efficiency requires the use of monochromatic incident photon beams, which are not possible to obtain by conventional X-ray tubes. The method proposed for this work consisted of using the fluorescent lines of different materials to constitute monochromatic beams to evaluate the corresponding relative responses. In the first step, the beam coming from the X-ray tube is used to irradiate samples of pure elements. Then, the secondary emitted characteristics photons are used to irradiate the flat panel.

In this context, the measurements that aimed to characterize quantum efficiency were performed using quasi-monochromatic radiation produced by the X-ray fluorescence in high-purity samples of different elements: *Se*, *Zr*, *Rh*, *Ag*, *Sn*, *Te*, *Ba*, *Se* and *Sm*. The K_α and K_β emission lines of these elements are in the range of 10–50 keV. Additionally, a radioactive sample of ^{241}Am was used to perform the irradiation with its intense 59.54 keV gamma line. Radiation produced in the samples was used to irradiate a small region of the VARIAN® PaxScan 2020+ flat panel, thus recording an *S* signal, calculated as the total amount of counts for each pixel being studied. A solid-state detector *CdTe* XR-100 Amptek® was used to measure, in the same position, the spectrum of the radiation generated by X-ray fluorescence and arrived at the specific position under study. Then, it becomes straightforward to determine the total photon flux *N* by direct integration of the recorded spectrum. The effective energy of the spectrum E_{ef} was calculated according to expression (7):

$$E_{ef} = \sum_{i=1}^{N} \rho(E_i) E_i \tag{7}$$

where the sum is extended to all energy channels (E_i), each one corresponding to recorded signal $\rho(E_i)$.

Then, the total amount of photons actually detected by the flat panel (N_f) is proportional to the recorded signal *S*. The corresponding quantum efficiency *QE* in terms of the effective energy of the incident radiation is given by expression (8):

$$QE(E_{ef}) = \frac{N_f}{N} = k\frac{S}{N} \tag{8}$$

where *k* is a proportionality constant independent of the energy E_{ef}. This parameter is obtained by fitting experimental results, using the calibrated *CdTe* solid-state detector as reference. The somewhat limited but still useful information provided by the manufacturer regarding the fact that the range of optimal efficiency of the detector for conventional X-ray tubes starts at approximately 60 kVp was taken into account. In this context, it was proposed to consider that, as a first approach, *QE* becomes practically 1 for beams harder than 40 kVp. But, of course, considering some upper limit, 150 kVp, approximately, as might be interpreted from the information provided by the manufacturer.

Preliminary results showed that the *QE* of the VARIAN® PaxScan 2020+ flat panel decreases rapidly for energies below 10 keV.[19,20] Therefore, the presence of secondary non-dominant X-ray fluorescence lines, lower than 10 keV, (as *L* and *M* lines) will not significantly affect the response of the system. According to typical detection responses, the *Error Function* provides an adequate description of the efficiency trend.[11] Hence, it was proposed to perform the corresponding fit of *QE*, as indicated in expression (9):

$$f(x) = \frac{1}{2}\,(ERF(ax - b) + 1) \tag{9}$$

where the values of the parameters *a* and *b* are obtained by fitting of experimental data. The method of fitting was based on nonlinear minimization of least squares, provided by the MatLab® platform.

Experimental setup

The X-ray imaging line is provided with a conventional X-ray tube with a tungsten (*W*) anode and thermoionic material in cathode. The Siemens Kristalloflex generator of maximum 3 kW power operates with a range of accelerating voltages from 20 to 60 kVp, as shown in Fig. 1, and cathode currents ranging from 5 to 60 mA. These values were used to define lower and upper limits for the range of interest during experimental determination of detector efficiency. The emission tower consists of four windows aligned with the maximum intensity directions of Bremsstrahlung, and it has a carousel of filters, including *Zr*, *V*, *Mn*, *Ni*, *Fe* and open beam among others.

The detection system of the X-ray imaging line is the flat planel VARIAN® Paxscan 2020+ Amorphous Silicon Digital X-Ray detector. As the name indicates, it contains an *Si* receptor and a *CsI* scintillator. This is the sampling system that works by discretization of a continuum in a 2D arrangement of pixels (nominal pixel pitch of 194 μm, as reported by manufacturer). This effect appears because the detector is composed of an arrangement of micro-photomultipliers. The process of discretization can be performed up to a certain limit related to the minimum spatial

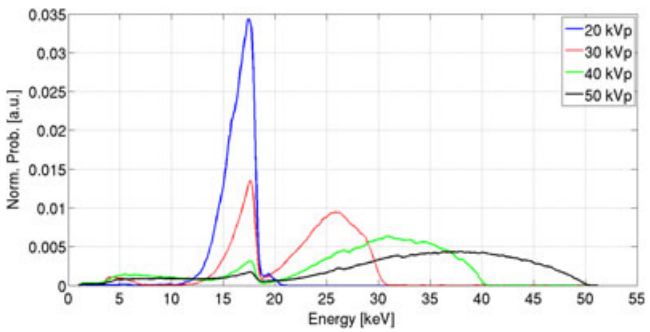

Figure 1. Example of spectra measured at the X-ray imaging line acquired with the *CdTe* XR-100 Amptek® (normalization was selected to total accounts).

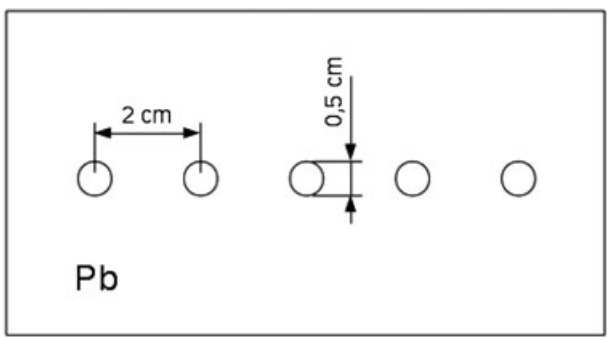

Figure 2. Sketch of collimation system used for the measurements of spatial uniformity of detector response. The lead sheet, 3 mm thick, has five circular (5 mm) holes 20 mm spaced.

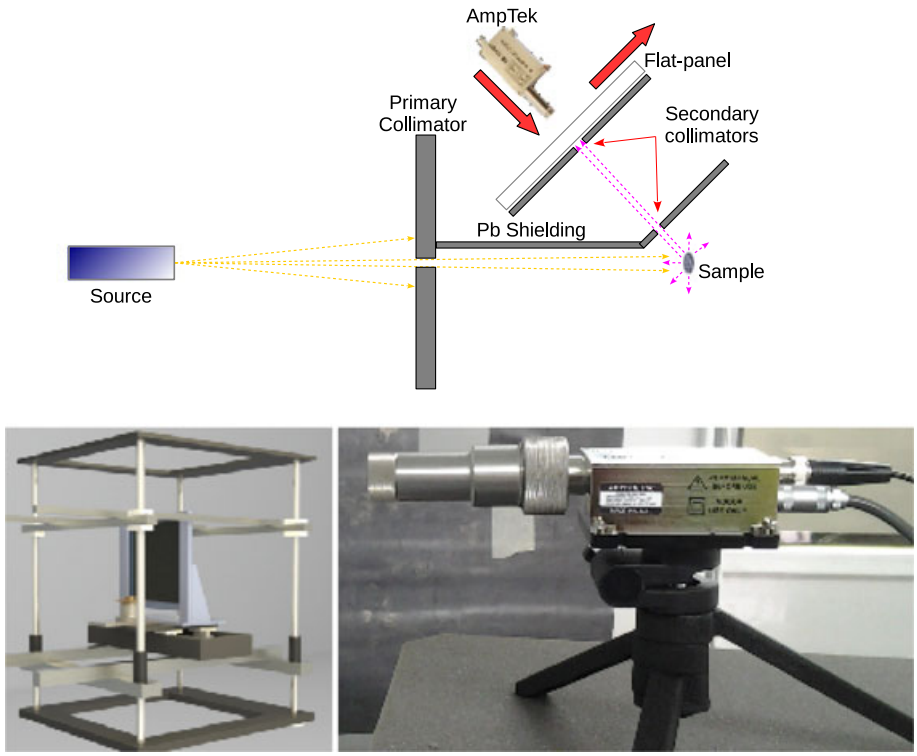

Figure 3. Sketch of setup used for the measurements of quantum efficiency. Flat panel (bottom left) and CdTe (bottom right) detectors are exchanged to measure in position behind the collimator indicated as *AmpTek* (top).

resolution of the detector, and possibly, the user's perception of a contrast limit. Care has been taken when adjusting dynamic range of the detector, with the aim of getting the best contrast possible, and the correct statistics in calculations involving the images taken. Taking into account the operating mode of the detector, an offset calibration is needed before each set of three measurements performed in every hole of the collimator. This is to correct the results for temperature and frame rate inaccuracies. The software viva provided by the manufacturer allows to generate the offset image and subtract it automatically to the measurements.

Figure 2 shows a sketch of the collimation system used for the determination of the spatial uniformity of detector response.

An extra collimation was added to each one of the holes in the lead slab consisting of a tungsten ring, 10 mm diameter and 1 mm thick, with central holes of different, calibrated diameters: 2000, 1000, 400, 200 and 100 μm. The collimation rings were positioned concentrically with the holes of the lead slab. The collimation system was positioned immediately before the flat panel detector, according to the 'beam view'. The distance between X-ray source and flat panel detector was fixed to 200 cm. This setup was designed for the measurements of *PSF*.

The use of *Pb* and *W* is supported by NIST[2] values of attenuation coefficient for photons of energies in the range of interest, virtually eliminating the signal outside the *PSF* diameter.

The collimation system was placed on top of the sensitive region of the detector, and then it was moved down displacing the axis of the holes. In the first set of measurements, the axis of the holes was 1.5 cm below the top limit of the sensitive region. The rest of this region was covered with lead sheets of 1 mm width. Except for the holes aimed to be measured, the rest of them were carefully covered with lead during irradiation, to avoid spurious signal in the *PSF* delicate measurement.

Once *MTF* were obtained for the various positions of measurement in the detector, a fitting process by means of Gaussian model was implemented, as indicated in expression (10):

$$f(x) = a\,e^{-bx^2} + c \tag{10}$$

Measurements of quantum efficiency were performed using the setup sketched in Fig. 3.

The method uses two detectors: the flat panel and a solid state detector capable of discriminating different energy channels with very high-energy resolution, better than 0.01 keV. It must be emphasized that the quantum efficiency of the *CdTe* XR-100 Amptek® detector is provided by the manufacturer, ensuring almost perfect sensitivity in the whole range of interest for this work.

Incident X-rays coming from the X-ray tube excite samples of high purity producing the subsequent X-ray fluorescence, which is isotropically emitted. Measurements are recorded in position indicated by *AmpTek* in Fig. 3. Some photons of the fluorescence, mainly constituted by K_α and K_β lines, go through the collimator hole, and then they are recorded by the detector positioned in that location. After verification of stability of photon fluence produced by X-ray tube, 99.37%, it is justified to use the same time acquisition windows for both detectors, or to incorporate the corresponding normalization for further correlation purposes is justifiable.

[2] **N**ational **I**nstitute of **S**tandards and **T**echnology, http://www.nist.gov/

Results and discussion

Preliminary measurements of the detection response for the linear array of collimators (response profile) of different inner diameters are reported in Fig. 4.

As can be appreciated, the collimator hole of smallest diameter providing acceptable signal-to-noise ratio is the 200 μm collimator. This effect was expected because of the small, but not negligible, beam divergence. Thus, once accurate alignment is warranted, the recorded signal for the 100 μm diameter collimator was high enough to be used for further measurements of *PSF*. Calculation of total counts recorded for each collimation diameter was performed averaging both possible positions of the lead collimator, front and reverse positioning. This process was useful to account for possible differences in intensity across the beam. The obtained results are reported in Fig. 5.

These results are compatible with at least two potential effects. The first one regards the possibility of non-uniform beam intensity; whereas the second is related to the divergence of the beam. Regardless these situations, the intensity modulation due to collimator diameter is the same in both cases, and *MTF* checks the relative intensity. Therefore, gradient corrections will not be necessary. This highlights how powerful the method of *OTF* is, not depending in this case on non-homogeneous properties of the physical system.

During the experiments, the X-Ray tube was set at 40 kVp so that the maximum energy of the photons of the beam was 40 keV (refer to the green line in Fig. 1 for the X-ray spectrum at 40 kVp). The electric current in the cathode was set to 10 mA. These magnitudes were chosen so that the dynamic range of the detector was covered. For eliminating low-energy components of the beam, which only contributes with noise on the images, 1 mm of aluminum (*Al*) was used as filter, and the carousel filter of the tube itself was set in Zirconium (*Zr*). Images were acquired during 30 s.

Figure 6 shows a typical experimentally measured *PSF*.

Figure 7 shows the fitting of various *MTF* for one of the positions of measurement in the detector. As shown, the fitting was performed using a model function of Gaussian shape, as explained previously.

For this set of measurements, the obtained value of cutoff frequency is $f_0 = (1.6 \pm 0.1)\ \frac{lp}{mm}$. The corresponding uncertainty was calculated through usual propagation, starting from the error of the fitting, and moving forward to the statistical error of the average over the three measurements.

In Fig. 8, each of the thirty-five points covering the net region of detection can be seen, with its corresponding statistics. The mean value of overall measurements gives a cutoff frequency value of $f_0 = (1.4 \pm 0.3)\ \frac{lp}{mm}$. This in turn leads to a minimum size measurable with the detector of (357 ± 14) μm, greater than pixel pitch, as may be expected. The error was obtained from the statistical uncertainties and the variance of the average calculation.

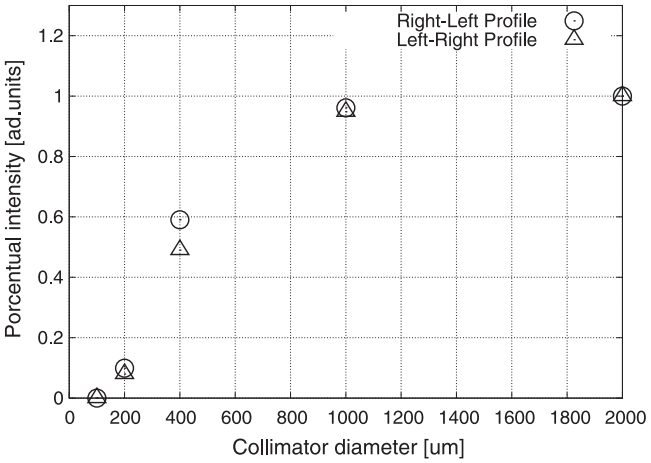

Figure 5. Relative intensity measured for the aligned collimators.

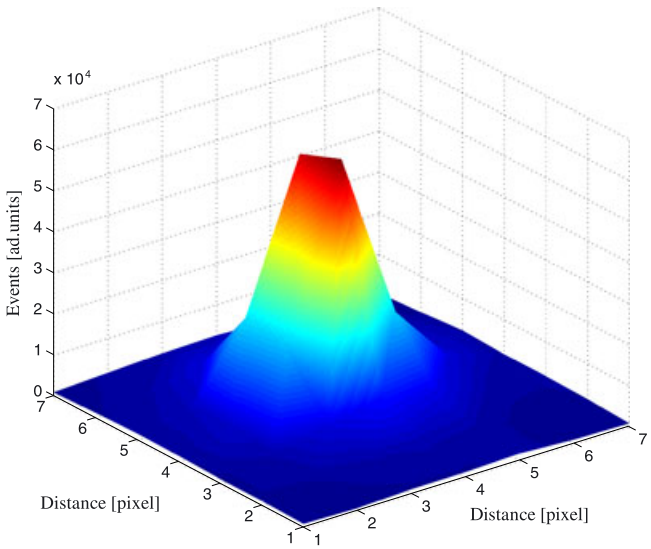

Figure 6. Point spread function measured over one region of the flat panel.

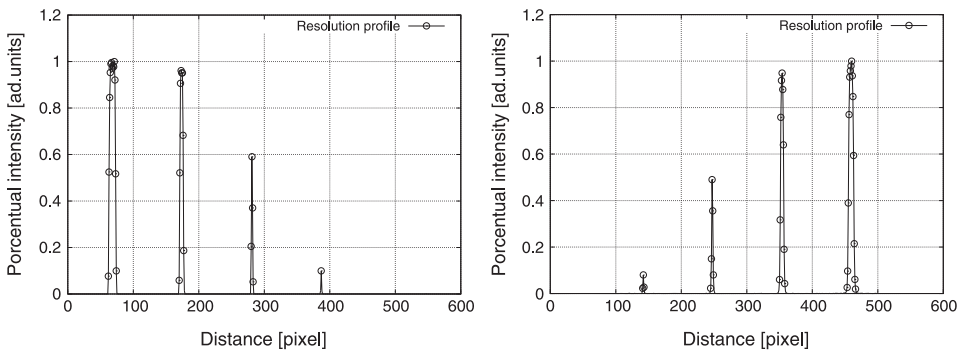

Figure 4. Examples of response profiles for the linear array of collimators positioning the lead collimator in both positions, front (left) and reverse (right).

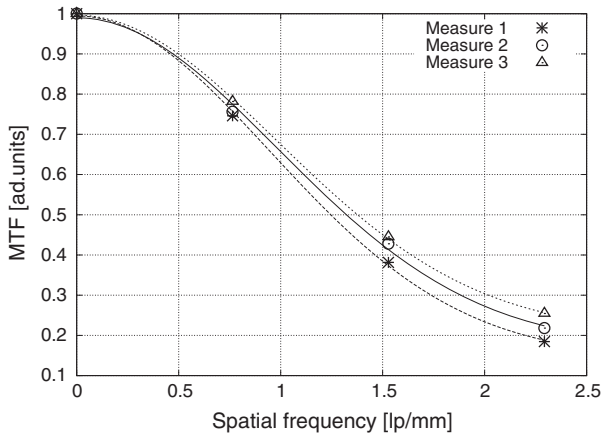

Figure 7. Typical behavior of modulation transfer function fitting for three independent measurements over one arbitrary point of flat panel detector.

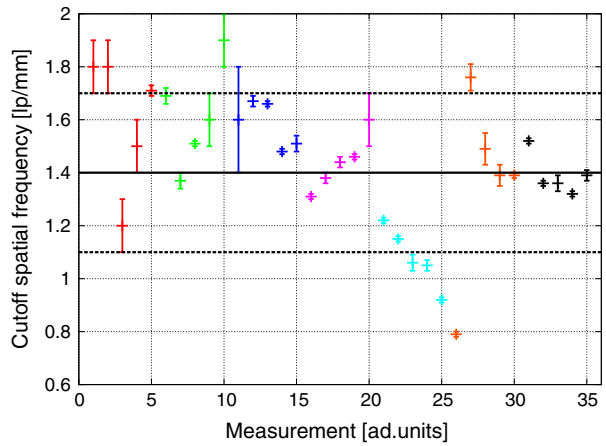

Figure 8. All measurements compared with the mean value calculated. Different colors indicate the seven different rows in the array of points where modulation transfer function was evaluated.

The mean value and corresponding uncertainty show the band of expected spatial resolution for the whole sensitive region. Counting how many of the measurements fall inside the band, the spatial resolution uniformity in the complete sensitive region was determined, obtaining 77 % of measurements inside the error bands. Restricting the analysis to a central region of 100×100 mm^2, the corresponding uniformity is 94%. Actually, this value should be considered to be more representative as a practical characterization of the detector for imaging purposes in typical setups in the LIIFAMIR$^{\textcircled{X}}$ μCT imaging line. The lack of perfect uniformity may be overcome for μCT applications by means of suitable corrections based on the map of relative responses.

Figure 9 shows the obtained results for the quantum efficiency of the VARIAN® PaxScan 2020+ flat panel detector.

During the fitting process for the *QE*, it was taken into account that the corresponding *QE* for the quasi-monochromatic photon beam produced by ^{241}Am was $QE(56.07\,\text{keV}) = 0.98$. This assumption, consistent with information provided by the manufacturer regarding the fact that the range of optimal efficiency of the detector for conventional X-ray tubes starts at approximately 60 kVp was required in order to assess an asymptotic trend for the

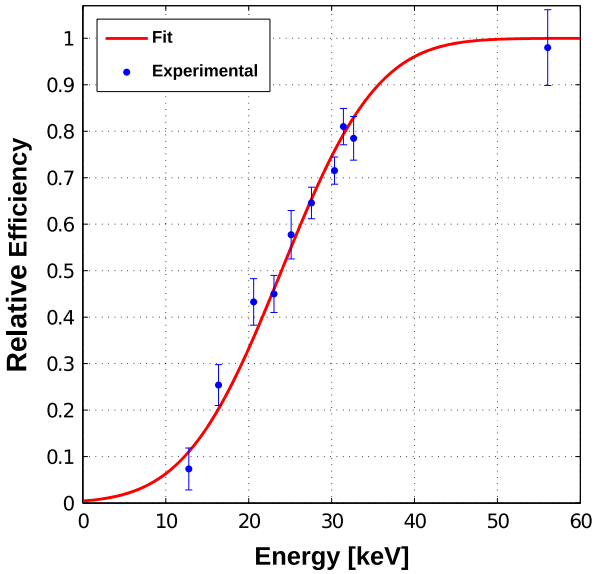

Figure 9. Efficiency of VARIAN® PaxScan 2020+ flat panel: experimental measurements (blue points) and corresponding fit (red line).

mathematical fit. However, it was corroborated that changing this parameter, in the range $QE(56.07\,\text{keV}) \in [0.95, 1]$ range, before fitting produced modifications in the values of parameters *a* and *b* of less than 5 % in both cases. The obtained values for the fitting parameters are $a = 8,044 \times 10^{-5}$ and $b = 1.958$, with correlation coefficient $R^2 = 0.99$.

Conclusions

The VARIAN® PaxScan 2020+ flat panel detector was characterized following rigorous experimental methods. The minimum size that can be distinguished by the detector is approximately twice the pixel pitch. This value should be taken into account for the quantitative capacity of detection. The results obtained showed that the uniformity of the sensitive region is high enough to support the use of the detector for more accurate measurements other than looking at a sample to make diagnostics.

Regarding the *QE* of the VARIAN® PaxScan 2020+ flat panel, it was possible to determine its behavior as a function of the corresponding effective energy of the incident radiation, thus obtaining a suitable assessment of $QE(E)$ for energy E in [10, 60] keV, approximately. This information, commonly not provided by the manufacturer, is absolutely necessary in order to perform any kind of reliable quantification using this detector. As a final result of the efficiency determination, a usable function of energy has been found, completely covering the energy range of interest for the operation of the X-ray tube of the X-ray imaging line. This might be used, for example, to correct image determination of absorption coefficient if the beam intensity has been measured, by making the suitable convolution of the recorded images.

Acknowledgements

This study was partially financed by CONICET by means of the Project ESPORA I - PIP 11220130100658CO and also by SeCyT-UNC by means of project ISIDORA II A-05/B527. The authors would like to thank Universidad Nacional (UNA), Heredia, Costa Rica, for the financial support (JB-C 0612-2014) of the PhD studies of

D. Chacón. The authors are also grateful to the Masters Program in Medical Physics of Universidad de La Frontera for supporting this project.

References

[1] S. Vedantham, A. Karellas, S. Suryanarayanan, D. Albagli, S. Han, E. J. Tkaczyk, C. E. Landberg, B. Opsahl-Ong, P. R. Granfors, Levis I., *et al.*, Full breast digital mammography with an amorphous silicon-based flat panel detector: physical characteristics of a clinical prototype, *Med. Phys.* **2000**, *27*, 558–567.

[2] S. Bartling, O. Majdani, R. Gupta, T. Rodt, C. Dullin, P. Fitzgerald, H. Becker, Large scan field, high spatial resolution flat-panel detector based volumetric CT of the whole human skull base and for maxillofacial imaging, *Dentomaxillofacial Radiol.* **2014**, *36*, 317–327.

[3] R. Baba, K. Ueda, M. Okabe, Using a flat-panel detector in high resolution cone beam CT for dental imaging, *Dentomaxillofacial Radiol.* **2014**, *33*, 285–90.

[4] J. Siewerdsen, D. Moseley, S. Burch, S. Bisland, A. Bogaards, B. Wilson, D. Jaffray, Volume CT with a flat-panel detector on a mobile, isocentric C-arm: pre-clinical investigation in guidance of minimally invasive surgery, *Med. phys.* **2005**, *32*, 241–254.

[5] R. I. Berbeco, S. B. Jiang, G. C. Sharp, G. T. Chen, H. Mostafavi, H. Shirato, Integrated radiotherapy imaging system (IRIS): design considerations of tumour tracking with linac gantry-mounted diagnostic X-ray systems with flat-panel detectors, *Phys. Med. Biol.* **2004**, *49*, 243.

[6] B. Sorcini, A. Tilikidis, Clinical application of image-guided radiotherapy, IGRT (on the varian OBI platform), *Cancer/Radiothérapie* **2006**, *10*, 252–257.

[7] R. R. of the International Commission on Radiological Protection, *ICRP Publication 26*, Pergamon Press, Oxford, **1977**.

[8] H. Geijer, K.-W. Beckman, T. Andersson, J. Persliden, Image quality vs radiation dose for a flat-panel amorphous silicon detector: a phantom study, *Eur. Radiol.* **2001**, *11*, 1704–1709.

[9] F. H. Attix, *Introduction to radiological physics and radiation dosimetry* (1st edn), Wiley-VCH, Madison, Wisconsin.

[10] W. R. Leo, *Techniques for Nuclear and Particle Physics Experiments* (2nd edn), Springer-Verlag, Berlin - Heidelberg.

[11] G. F. Knoll, *Radiation Detection and Measurement*, John Wiley & Sons, New York, NY, **2010**.

[12] C. E. Metz, K Doi, Transfer function analysis of radiographic imaging systems, *Phys. Med. Biol.* **1979**, *24*, 1079–1106.

[13] G. Arfken, H. Weber, *Mathematical Methods for Physicists* (6th edn), Elsevier Academic Press, San Diego, California, **2005**.

[14] K. F. Riley, M. Hobson, S. Bence, *Mathematical Methods for Physics and Engineering* (2nd edn), Cambridge University Press, Cambridge, UK, **2002**.

[15] A. V. Oppenheim, A. S. Willsky, S. H. Nawab, *Signals & Systems* (2nd edn), Prentice-Hall, Inc., Upper Saddle River, NJ, USA, **1996**.

[16] A. Jerri, The Shannon sampling theorem its various extensions and applications: a tutorial review, *Proc. IEEE* **1977**, *65*, 1565–1596.

[17] R. G. Figueroa, E. Lozano, F. Belmar, D. Alcaman, A. von Bohlen, C. A. B. Oliveira, A. L. M. Silva, J. F. C. A. Veloso, Characteristics of a robust and portable large area X-ray fluorescence imaging system, *X-Ray Spectrom.* **2014**, *43*, 126–130.

[18] S. W. Smith, *The Scientist and Engineers Guide to Digital Signal Processing* (2nd ed.), California Technical Pub., California, **1999**.

[19] E. Samei, J. M. Flynn, G. H. Chotas, T. J. III Dobbins, DQE of direct and indirect digital radiography systems, *SPIE Med. Imag.* **2001**, *4320*, 189–197.

[20] P. Granfors, R. Aufrichtig, Performance of a 41 ×41 — cm^2 amorphous silicon flat panel X-ray detector for radiographic imaging applications, *Med. Phys.* **2000**, *27*, 1324–1331.